

Article

A New Load-Transfer Factor to the Slipping Analytical Formulation in Axially Loaded Piles

Kelvin Lo *, Erwin Oh , Darren Newell and Choo Yong

School of Engineering and Built Environment, Griffith University, Southport, QLD 4222, Australia; y.oh@griffith.edu.au (E.O.); darren.newell@griffithuni.edu.au (D.N.); choo.yong@griffith.edu.au (C.Y.)
* Correspondence: losze2012@gmail.com

Abstract: The load-transfer factor (ζ) in the concentric cylinder approach is often used in analytical formulation in axially loaded piles. The factor is a constant value (in a given pile slenderness ratio and soil condition) devised under the elastic and ‘pre-failure’ perfect pile–soil bonding conditions (a non-slip analytical model). Given most numerical methods have already considered the pile–soil slipping in the ‘pre-failure’ stage, the limitations of non-slip analytical models have recently been discussed, and slipping analytical models have been recommended. Therefore, this research aims to investigate the load-transfer factor in slipping analytical models. This paper reviews that the factor in slipping analytical models is only constant in linear elastic and some Gibson soil conditions. Beyond these conditions, the factor varies as the pile-head load increases in some cohesionless soils. Adopting the existing constant factor in slipping analytical models will deviate the load–displacement results, as supported by numerical results. Therefore, a new equation is proposed to the load-transfer factor, and a new analytical method is proposed by varying the load-transfer factor during loading for improvement. Results presented in this paper demonstrate improved load–displacement results.

Keywords: load-transfer factor; finite element; analytical method; axially loaded piles



Citation: Lo, K.; Oh, E.; Newell, D.; Yong, C. A New Load-Transfer Factor to the Slipping Analytical Formulation in Axially Loaded Piles. *Geotechnics* **2022**, *2*, 171–190. <https://doi.org/10.3390/geotechnics2010008>

Academic Editors: Qi Wang, Bei Jiang, Xuezhen Wu and Hongke Gao

Received: 28 January 2022
Accepted: 12 February 2022
Published: 17 February 2022

Publisher’s Note: MDPI stays neutral with regard to jurisdictional claims in published maps and institutional affiliations.



Copyright: © 2022 by the authors. Licensee MDPI, Basel, Switzerland. This article is an open access article distributed under the terms and conditions of the Creative Commons Attribution (CC BY) license (<https://creativecommons.org/licenses/by/4.0/>).

1. Introduction

The concentric cylindrical approach was originally proposed by Randolph and Wroth [1] and is often adopted by researchers (such as Kraft et al. [2], Alawneh [3], Pando et al. [4], Wang et al. [5], Zhang et al. [6], Cheng et al. [7]) to determine the analytical load-response behavior of axially loaded piles. The approach relies on a load-transfer factor (ζ), which is a function of the pile radius (r_0) and r_m (Equation (1)). The r_m value is a radial distance at which the shear stress becomes diminishingly small and negligible. In the past, the ζ factor was devised under elastic mediums in non-slip analytical models, as described in Lo et al. [8]. Recently, the limitations of non-slip analytical models have been discussed in Wang et al. [5], Lo et al. [8], Sheil and McCabe [9], Boonyatee and Lai [10], and slipping analytical models were recommended. In this study, the ζ factor in slipping analytical models is reviewed using finite element (FE) analyses of homogeneous and vertically inhomogeneous (Gibson soil, linear increase in the soil shear modulus (G) with depth) soils under the linear elastic and Mohr-Coulomb (MC, linear-elastic-perfectly-plastic) models. Results show that constant values are valid in elastic soils and soils with a constant ratio of shear modulus to the ultimate shear strength (τ_{ult}) in the Gibson condition. However, in certain cohesionless soils, ζ is found to vary as the pile-head load increases and a new equation for ζ is proposed to account for this. Furthermore, a new analytical method is proposed to determine the load–displacement curve. An automated procedure was employed by combining *Python* codes and *VBA* (Visual Basic Application) macro to control the FE analysis (*PLAXIS 2D*) and perform the analytical calculations.

$$\zeta = \ln\left(\frac{r_m}{r_0}\right) \quad (1)$$

2. Background

2.1. Load-Transfer Factor (ζ)

In the concentric cylindrical approach, the deformation of the soils surrounding the pile shaft is idealized as shearing of concentric cylinders [1]. Pando et al. [4] commented that the concentric cylinder approach provides a good approximation of the deformation patterns obtained using more rigorous analyses such as finite element analysis. Randolph and Wroth [1] demonstrated that an estimate of vertical displacement of soil at the pile shaft (w_s) is given by Equation (2), where τ_o is the shear stress at the pile shaft. Initially, Randolph and Wroth [1] evaluated ζ by comparing the settlement profile of the surrounding soil at the mid-depth level of the pile to that calculated from integral equation analysis, for a pile slenderness ratio of $L/r_o = 40$ (where L is the pile length). The ζ factor was further extended by Randolph [11] to improve the accuracy of predicting the load-displacement behavior of both short and long piles by comparing to Poulos and Davis [12] and Carter and Kulhawy [13]. Guo [14] then used a more rigorous approach using the finite difference software *FLAC* to evaluate ζ in an elastic medium. The approach involved iteratively adjusting ζ until the pile-head stiffness matched both the analytical closed-form solution and the finite different numerical results.

$$w_s = \frac{\tau_o r_o}{G} \zeta \quad (2)$$

The general form of ζ is provided in Equation (3), where ν_s is the soil's Poisson ratio, and ρ is equal to the ratio of the shear modulus at mid-depth of the pile to that at the base. The constants, A and B used in Equation (3) have been determined by various researchers and are summarized in Table 1.

$$\zeta = \ln \left[A \rho (1 - \nu_s) \frac{L}{r_o} + B \right] \quad (3)$$

Table 1. Values for A and B (Equation (3)) under different literature.

Literature	A	B
(i) Randolph and Wroth [1]	2.5	0
(ii) Randolph [11]	2.5	5
(iii) Guo [14] ^A	2.1	1

^A An approximated value for deep homogenous layers with some loss of accuracy.

2.2. Pile–Soil Interface

As discussed by De Gennaro et al. [15], when considering pile-soil interaction, failure of the soil is characterized by the deformation of a thin soil lens (interface) orientated in the direction of the contract surface. Many researchers [15–21] have shown that assuming an interface along the pile shaft is essential in predicting pile behavior under loads. Sheil and McCabe [9] commented that most numerical methods have already included the pile–soil slipping behavior (pile–soil relative displacement) by introducing interface elements along the pile shaft in the numerical models. Coutinho et al. [18] emphasized that interface elements must allow for relative displacements between two bodies in contact or separated by a thin material layer. However, existing simplified analytical methods still assume ‘pre-failure’ conditions that imply perfect pile–soil bonding characteristics (non-slip analytical models).

This study adopted the formulation of interface elements in *PLAXIS 2D* to simulate the pile–soil interaction for use in the analytical method. Slipping is considered in terms of relative pile–soil displacement at the interface along the pile shaft. A virtual thickness is assigned to the interface, which is an imaginary dimension used in part to define its material properties. The coordinates of each pair of nodes at the pile–soil interface are

identical, which means that the interface has a zero thickness [22]. The pile–soil slipping (Δw) is governed by

$$\Delta w = w_p - w_s = \frac{\tau_o t_i}{G_i} \tag{4}$$

where w_p and w_s are the vertical displacement of pile and soil nodes at the interface, G_i is the shear modulus of the interface (calculated by an interface factor R_i^2 multiplying the soil shear modulus G), and t_i is the virtual thickness of the interface and calculated by a virtual thickness factor (default value = 0.1) times the global element size calculated from the model dimensions [22].

3. A Review of the Load-Transfer Factor by Finite Element Analysis

3.1. Model Verification

FE analyses using *PLAXIS* do not directly provide the ζ factor, however values for τ_o and w_p which are used in Equation (5) to evaluate ζ . Equation (5) is proposed in this study, which is a combination of Equations (2) and (4). Verification of this proposed method for evaluating ζ involved comparing values of ζ resulting from an FE model to those obtained from previously published values.

$$\zeta = \left(\frac{w_p G}{\tau_o r_o} - \frac{t_i}{R^2 r_o} \right) \tag{5}$$

The first step in developing the FE model used in this study involved optimizing it in terms of mesh size and the model boundaries. The effect of the mesh size and total height (H) of the modeled soil on resulting values of ζ is shown in Figures 1 and 2. From these figures, it can be seen that the effect is minimized when the r_e and H/L factors reach 0.35 and 6, respectively, for $L/r_o = 40$ and $G = 1923$ kPa. Similar results were obtained in other combinations among $L = 10$ to 30 m, $L/r_o = 20$ to 60, $H/L = 2$ to 8, and $G = 1.92$ to 11.54 GPa. Therefore, values of $r_e = 0.35$ and $H/L = 6$ were adopted for the FE model used in this study.

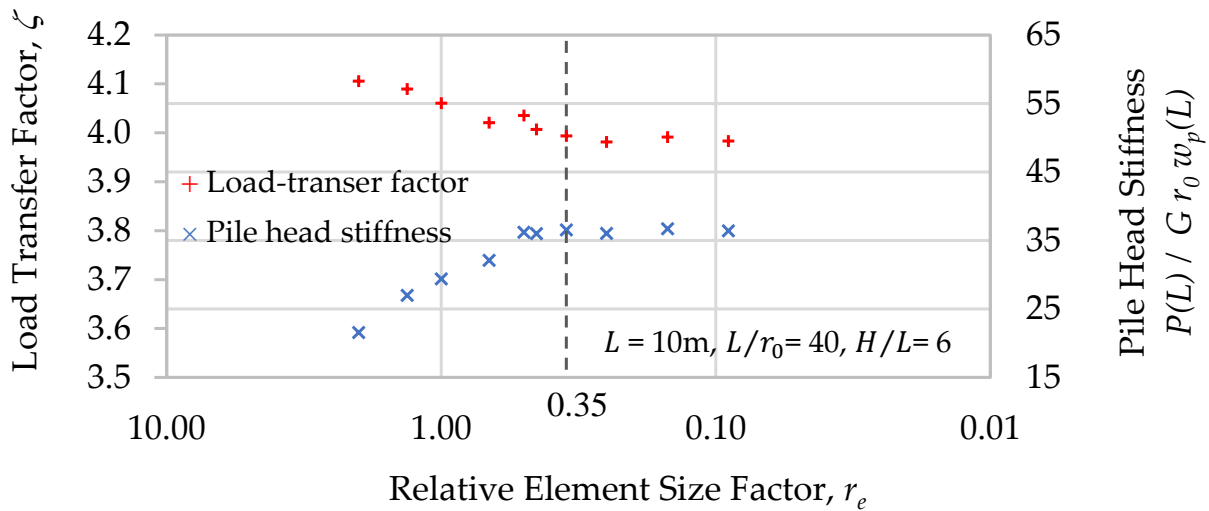


Figure 1. Load transfer factor and pile head stiffness versus relative element size factor.

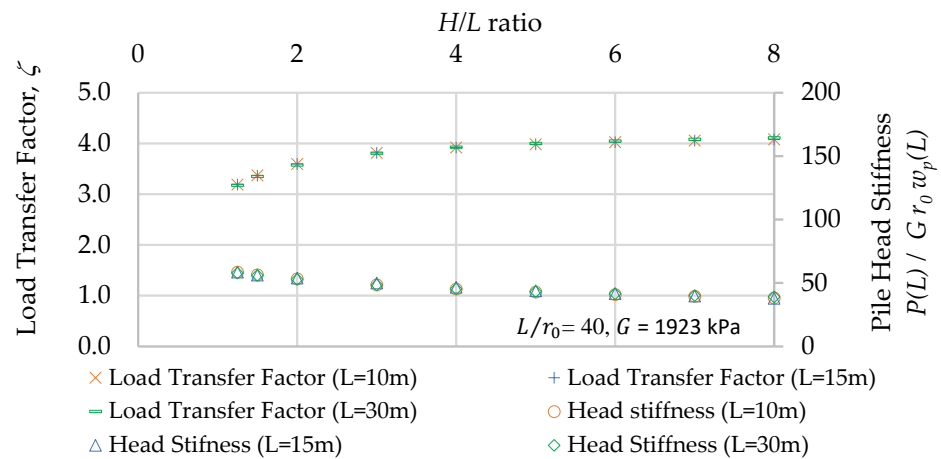


Figure 2. Load transfer factor and pile head stiffness, versus H/L ratio.

After determining the optimum mesh and boundary geometries, the FE model used in this study was verified by comparing the calculated ζ values using Equation (5) proposed in this study at the mid-depth level of the pile embedded in elastic soils, with values provided in Randolph [11]. Figure 3 demonstrates a high degree of correlation between ζ values calculated using Equation (5) and corresponding values provided by Randolph [11] (within approximately 2%).

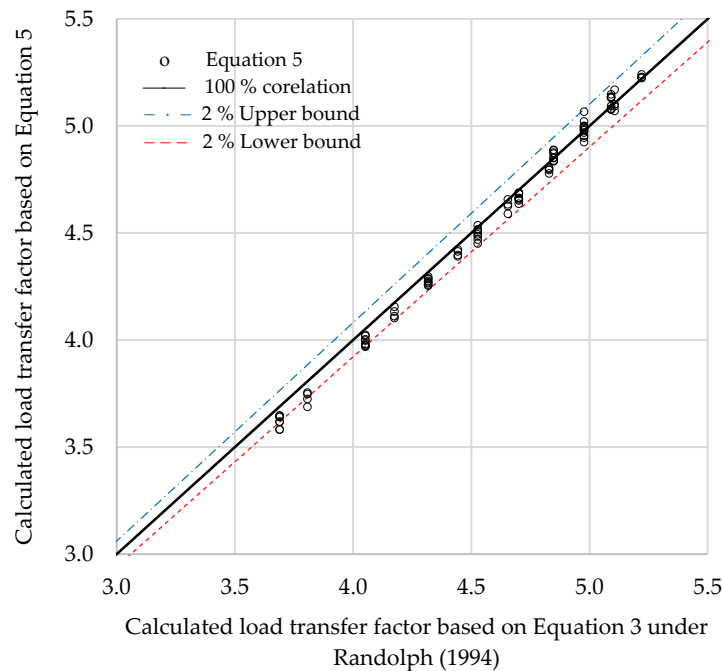


Figure 3. Load-transfer factors (ζ) from PLAXIS 2D versus equivalent ζ factors from Randolph [11], for about 100 cases ($L = 10\text{--}25$ m, $L/r_0 = 20\text{--}90$, $\nu_s = 0.2\text{--}0.3$, $G = 3.8\text{--}7.7$ GPa).

The adopted FE model was further verified by comparing to the analytical closed-form solution under the suggested ζ factor from Guo [14] for 24 cases ($L = 10\text{--}30$ m, $L/r_0 = 40\text{--}60$; $\nu_s = 0.2$, $G = 1.92\text{--}7.70$ GPa). Again, a high degree of correlation was obtained in all combinations. Figure 4 shows one of the typical results amongst the 24 cases analyzed. It compares the load–displacement curves at the pile head between the analytical formulation based on the load-transfer factor recommended from Guo [14] and the verified FE model in elastic soil.

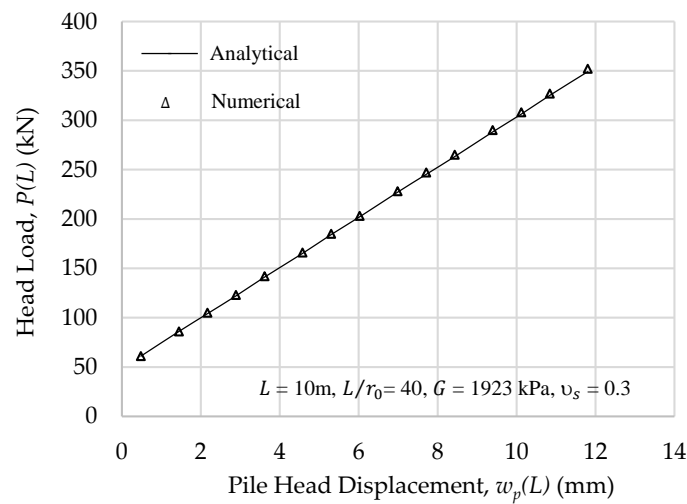


Figure 4. Pile head load (P) versus pile head displacement (w_p), comparison of the analytical closed-form solution suggested from Guo [14] and the adopted FE model in elastic soil.

3.2. A Review of the Load-Transfer Factor

An axially loaded pile was analyzed under tension and compression loads, using linear elastic (LE) and Mohr–Coulomb (MC) constitutive soil models in the FE model used in this study. Values for parameters used for modeling the pile comprised a diameter of 1.2 m and length of 15 m, with an elastic modulus (E_p) and Poisson ratio (ν_p) of 30 GPa and 0.15 respectively. The ζ value at the mid-depth level of the pile was reviewed (similar to Randolph and Wroth [1]) by substituting the shear stress and vertical displacement of the FE results into Equation (5). The mid-depth level was chosen on the presumption that it is least affected by boundary edge effects and discontinuities at the pile head and toe. Five different FE models (Table 2) were analyzed in both axial tension and compression:

- Model 1: Homogeneous, LE constitutive soil model.
- Model 2: Gibson (inhomogeneous), LE constitutive soil model.
- Model 3: Gibson (inhomogeneous), elastoplastic MC constitutive soil model with a constant G/τ_{ult} ratio where the entire pile–soil interface becomes plastic (reaching the ultimate shear strength, τ_{ult}) along the total pile length simultaneously.
- Model 4: Homogenous (modulus only), MC constitutive soil model with a fixed strength profile along the interface. The shear strength profile is an input parameter converted from initial overburden stress based on Das [23] to simulate cohesionless soil. It is a simplified version of Model 5.
- Model 5: Homogenous (modulus only), MC constitutive soil model with a variable strength profile along the interface. Soil strength is a function of the friction angle (input parameter) and the rotation of principal stresses (updated automatically as pile-head load increases).

Table 2. Summary of soil and interface parameters in different FE models analyzed.

MODEL	1C/1T	2C/2T	3C/3T	4C/4T	5C/5T
Soil model	LE	LE	MC	MC	MC
E_{ref} (kPa)	10,000	4000	4000	10,000	10,000
E_{inc} (kPa/m)	0	400	400	0	0
c_{ref} (kPa)	-	-	10	1	1
c_{inc} (kPa/m)	-	-	1	5.2	-
ϕ (°)	-	-	-	-	30

Note: ‘C’ and ‘T’ denote compression and tension loads; c_{ref} and c_{inc} are the shear strengths at the ground level and incremental value with depth, respectively for both the soil and interface; E_{ref} and E_{inc} are the stiffness at the ground level and incremental value with depth, respectively for both the soil and interface; ϕ is the friction angle of the soil.

Figure 5 shows that the estimated ζ factor in FE Model 1 (3.85 compared to 3.89) and Models 2 and 3 (3.51 compared to 3.57) closely align with values suggested by Randolph [11]. It can also be seen from Figure 5 that estimated ζ values are constant as the pile-head load increases in the LE models (Models 1 and 2) and for a Gibson soil with a constant ratio of G/τ_{ult} (Model 3).

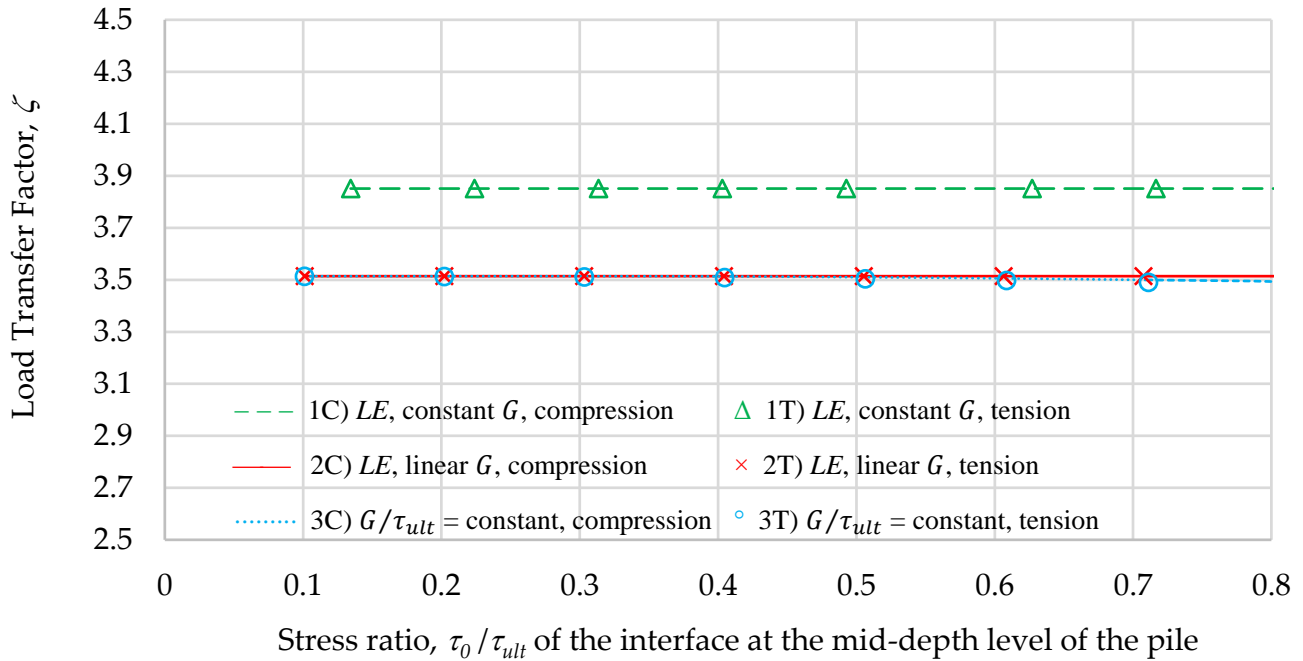


Figure 5. Load transfer factor versus stress ratio at mid-depth for Models 1 to 3.

The constant value of ζ estimated in Model 3 (Figure 5) is a result of the interface behaving linearly-elastic as the pile load increases up until a certain load where it reaches a plastic state along its entire length simultaneously. It can be explained by the analytical theory supported by the FE results. Randolph and Wroth [1] commented that the distribution of shear stress along the pile shaft is similar to $\tau_i(z) = k_i(b + z)$ for soil shear modulus in the form of $G(z) = m(b + z)$ as shown in Figure 6, which can be expressed as

$$\frac{\tau_i(z)}{G(z)} = \frac{k_i(b + z)}{m(b + z)} = \frac{k_i}{m} \tag{6}$$

The term k_i in Equation (6) is a constant for load step i , where PLAXIS divides each calculation phase into several calculation steps, and load is applied in small proportions called load steps [22]. In Model 3, if m , b , and K are constants, the ratio of soil shear modulus to strength is constant and is equal to

$$\frac{G(z)}{\tau_{ult}(z)} = \frac{m(b + z)}{K(b + z)} = \frac{m}{K} \tag{7}$$

The ratio of shear stress ($\tau_i(z)$) to shear strength ($\tau_{ult}(z)$) along the shaft at load step i is a constant, which is confirmed from the FE results presented in Figure 7 and is expressed as

$$\frac{\tau_i(z)}{\tau_{ult}(z)} \approx \frac{k_i}{K} = constant \tag{8}$$

For load steps with $k_i < K$, the shear stress $\tau_i(z)$ at any pile depth is smaller than the ultimate value $\tau_{ult}(z)$ and the interface along the whole shaft remains in an elastic state. When $k_i = K$, $\tau_i(z)$ at any depth is equal to $\tau_{ult}(z)$ and the pile interface simultaneously reaches a plastic state along the entire pile length. Therefore, the estimated ζ factor is mainly the same as the linear elastic model. The near constant value for ζ can further be explained by the mathematical derivative of the shear strain (γ) with respect to z

$$\gamma'_i(z) = \frac{\partial \left[\frac{\tau_i(z)}{G(z)} \right]}{\partial z} = \frac{m(b+z) \frac{\partial(k_i(b+z))}{\partial z}}{m^2(b+z)^2} - \frac{k_i(b+z) \frac{\partial(m(b+z))}{\partial z}}{m^2(b+z)^2} \tag{9}$$

When Equation (9) is simplified, the first and second terms simplify to $k_i/m(b+z)$ which results in $\gamma'_i(z) = 0$. This results in the shear strain (γ_i) in a load step i being nearly constant along the pile shaft as shown in the FE results in Figure 8. The shear stress along the pile shaft in a load step i is defined as

$$\tau_i(z) = \gamma_i(z) * G(z) = \gamma_i(z) * m(b+z) \leq K(b+z) = \tau_{ult}(z) \tag{10}$$

Theoretically, the term $\gamma_i(z) * m$ in the above equation continuously increases with increasing pile head loads. Eventually, it reaches the ultimate value of K , and the whole pile interface becomes plastic simultaneously.

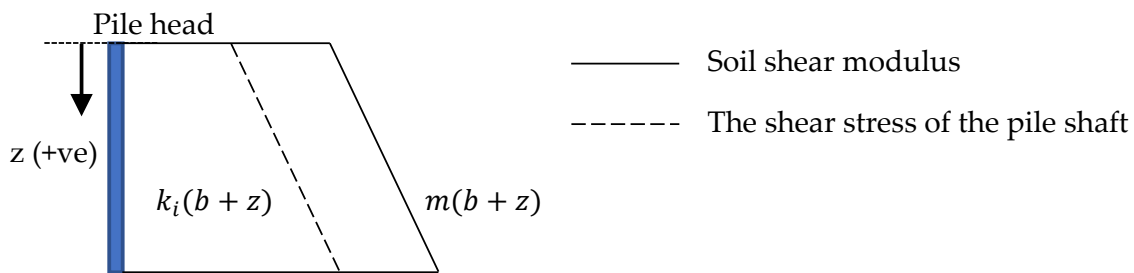


Figure 6. Shear stress and modulus profile along the pile shaft.

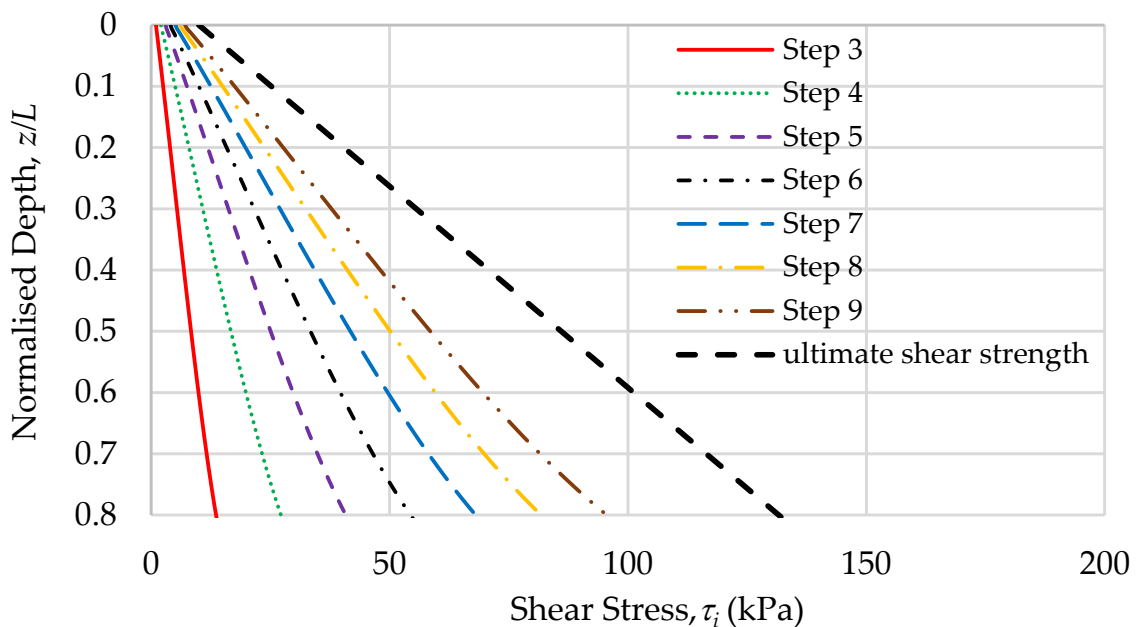


Figure 7. Normalized depth versus shear stress at the pile shaft in a load step, from FE analysis.

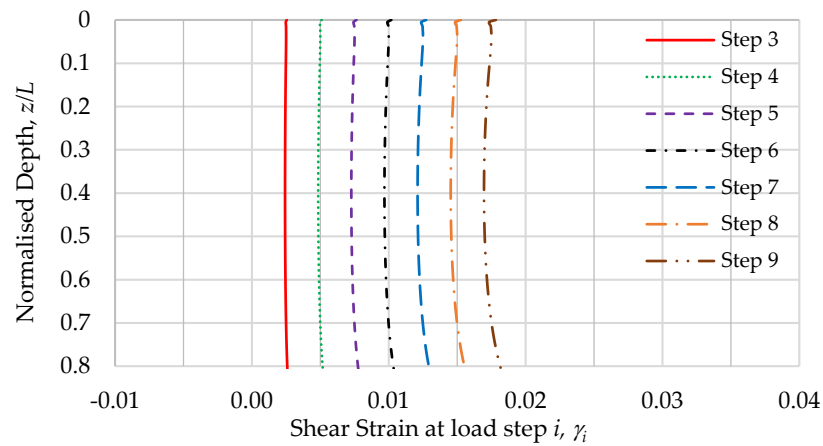


Figure 8. Normalized depth versus shear strain, from FE analysis.

Figure 9 demonstrates that the estimated value of ζ is no longer constant but changes as the pile-head load increases in the MC constitutive models (Models 4 and 5). This can be explained by rearranging Equation (2) ($w_s/\tau_0 = \zeta r_0/G$) in which the ratio of w_s/τ_0 is lesser than that in the elastic model (Model 1). It results from the reduction of soil movement adjacent to the pile shaft and the increase in τ_0 . When τ_0 reaches τ_{ult} the interface will exhibit plastic behavior. That is, it will continuously displace at the τ_{ult} value (Figure 10). The pile–soil plastic slip commences at the upper portion of the pile shaft and progressively develops down the pile shaft in Models 4 and 5. This phenomenon is explained in Lo et al. [8] and adopted by many researchers to simulate cohesionless soils. Once the pile–soil plastic slip has occurred, the rate of vertical soil movement adjacent to the pile shaft around the slip portion (upper portion) reduces. This effect releases the downward ‘pushing’ effect from the upper portion onto the soil below (in compression piles), and the upper portion restrains the vertical soil movement below (in tension piles). Consequently, the vertical soil displacement (w_s) below the slip portion is lesser in Models 4 and Model 5 compared to the elastic model (Model 1), as shown in Figure 11. However, the pile keeps moving as the pile head load increases, which results in larger pile–soil relative displacement ($\Delta w = w_p - w_s$) and therefore larger mobilized shear stress (τ_0) based on Equation (4) ($w_p - w_s = \tau_0 t_i/G_i$).

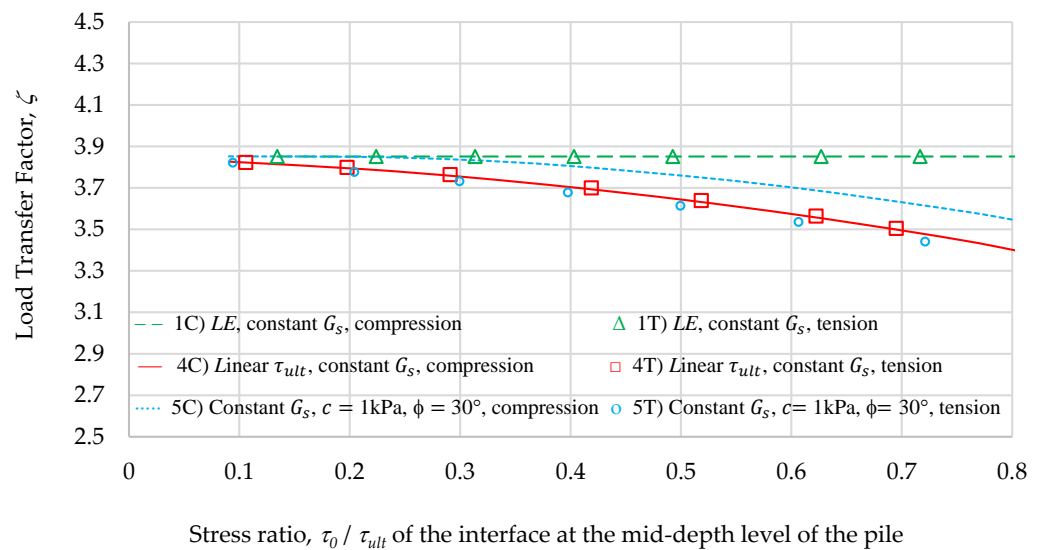


Figure 9. Load-transfer factor versus stress ratio at the mid-depth level of the pile as head load increases in Models 1, 4, 5.

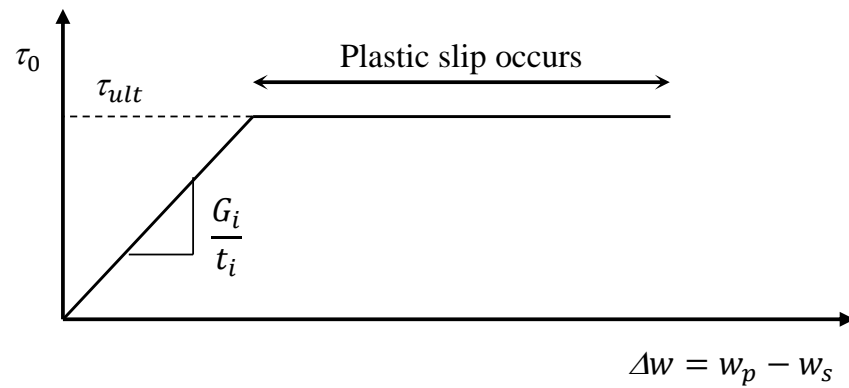


Figure 10. Shear stress versus pile–soil relative displacement.

Figure 9 demonstrates that during compression loading, the corresponding reduction of the estimated ζ factor in Model 5C ($c = 1$ kPa and $\phi = 30^\circ$) is lesser than the simplified Model 4C ($c = 1 + 5.2 z$ and $\phi = 0^\circ$). In contrast, during tension loading, the reduction in Model 5T ($c = 1$ kPa and $\phi = 30^\circ$) is slightly higher than the simplified Model 4T ($c = 1 + 5.2 z$ and $\phi = 0^\circ$), but very similar. The difference in ζ is due to the increase in mobilized shear strength along the pile shaft in Model 5C under compression loads and decrease in Model 5T under tension loads, as observed in O’Neill [24] and De Nicola and Randolph [25]. It results in the depth of pile–soil plastic slip ($L - iL$) being lesser in Model 5C and larger in Model 5T compared to the simplified Model 4 (supported by the FE results in Figure 12). As a result, the reduction of the ζ factor in Model 5C is lesser than Model 4C and the reduction in Model 5T is larger than Model 4T.

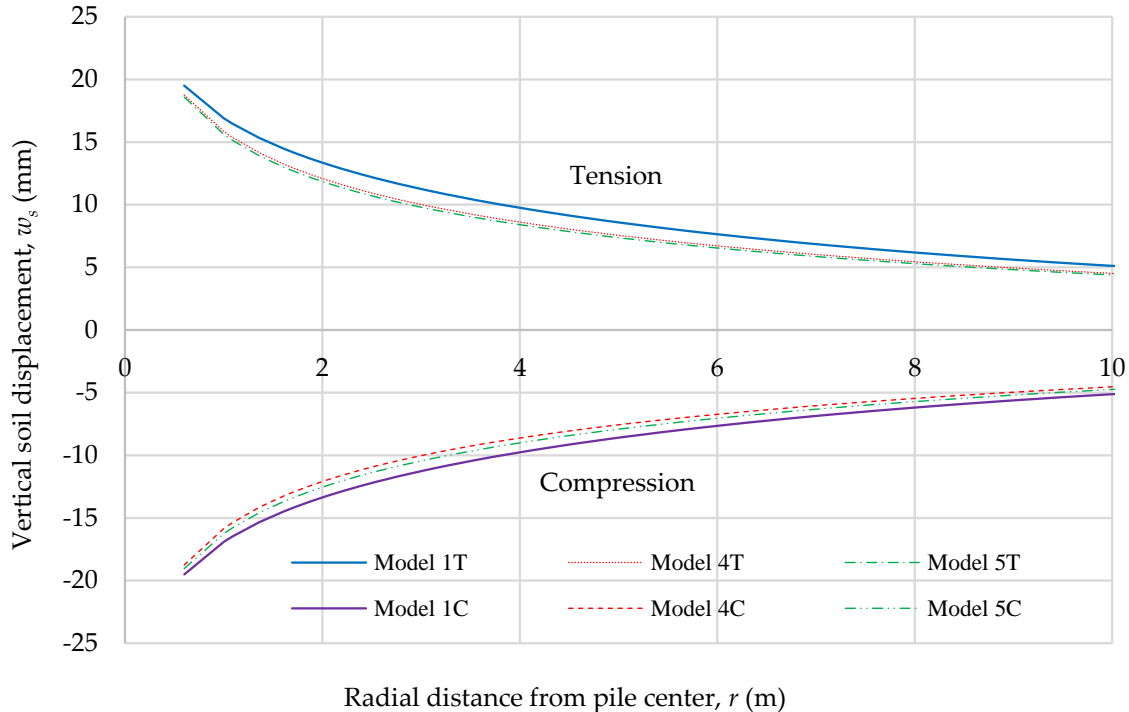


Figure 11. Soil displacement in the mid-depth level of the pile versus radial distance from pile center, from FE analysis.

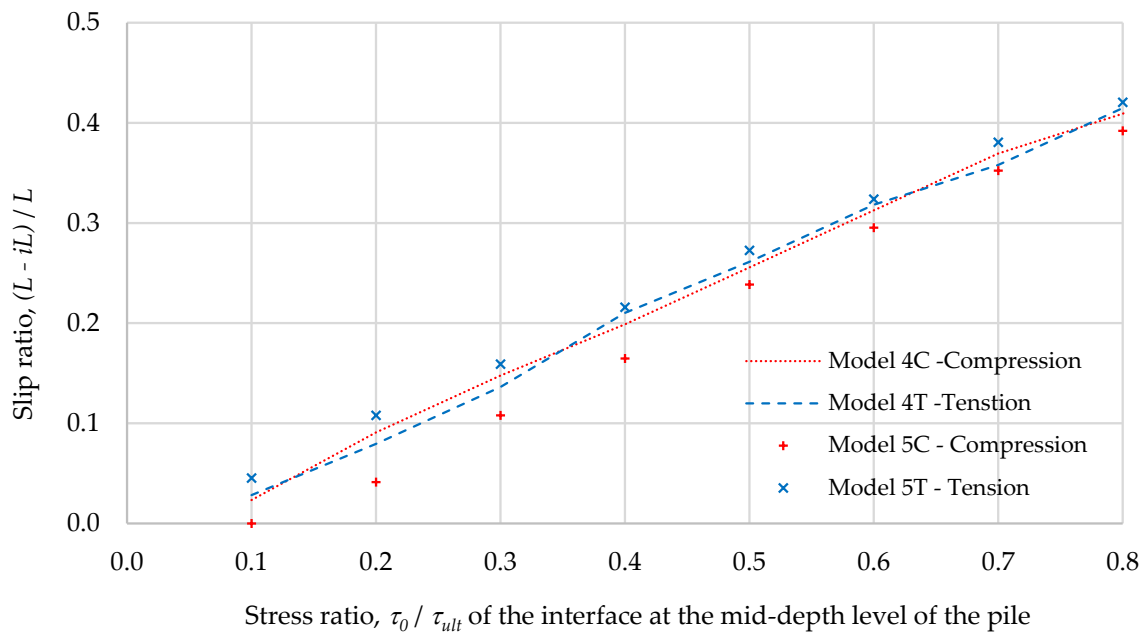


Figure 12. Slip ratio (slip depth to pile length) versus stress ratio at the mid-depth level of the pile.

Figure 9 shows that the estimated value of ζ in Model 4T (simplified model under tension loads) is very close to that in Model 5T. Therefore, Model 4T was adopted to simulate piles under tension loads in some cohesionless soils in the next section.

4. New Analytical Method and Improvement in the Load–Displacement Curve

This section considers the change in ζ when determining the load–displacement curve for some cohesionless soils. With the initial application of a tensile load to the pile, the whole interface remains elastic. As the tensile load increases, the plastic slip (Figure 10) of the soil–pile interface is first reached at the top of the pile. It progressively transcends downward to the toe (Figure 13b), where the whole interface becomes plastic. Many researchers (such as Misra et al. [26], Guo [14], and Meerdink et al. [27]) have adopted this elastoplastic form to model cohesionless soils.

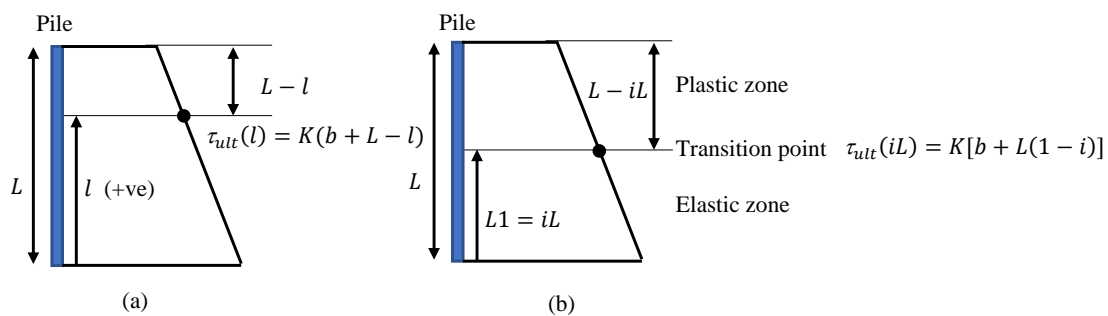


Figure 13. (a) Shaft strength profile, (b) transition between elastic and plastic portions.

4.1. Devising the Elastoplastic Analytical Solution

4.1.1. Elastic Component

The deformation of a pile under the pile elasticity theory and vertical force in equilibrium is shown in Equation (11). Where the l term in Equation (11) is the distance measured from the pile toe for piles under tension load, which is different from the z term used in the previous sections, which is distance from the pile head. The terms $P(l)$, $w_p(l)$ and $\tau_0(l)$ are

the pile axial load, pile axial displacement, and vertical shear stress at the pile shaft at a distance l from the pile toe, respectively. Finally, the λ term is equal to E_p/G .

$$\frac{\partial^2 w_p(l)}{\partial l^2} = \frac{1}{\pi r_o^2 \lambda G} \frac{\partial P(l)}{\partial l} = \frac{2}{r_o \lambda G} \tau_0(l) \tag{11}$$

If $w_s(l)$ is the vertical soil displacement at the pile shaft at a distance l from the pile toe, the vertical soil displacement (w_s) at the pile shaft can be combined with the concentric cylindrical equation (Equation (2)) and Equation (11), which yields

$$\frac{\partial^2 w_p(l)}{\partial l^2} = \frac{2w_s(l)}{r_o^2 \lambda \zeta} \tag{12}$$

Combining the interface equation and concentric cylindrical equation, Equations (4) and (2), respectively, results in

$$w_s(l) = w_p(l) \frac{r_o \zeta R^2}{r_o \zeta R^2 + t_i} \tag{13}$$

Combining Equations (12) and (13), yields the second-order differential equation

$$\frac{\partial^2 w_p(l)}{\partial l^2} = \frac{2 R^2}{r_o \lambda (r_o \zeta R^2 + t_i)} w_p(l) \tag{14}$$

By solving the second-order differential equation under the boundary conditions of $P(0) = 0$ and $w_p(0) = w_b$ at the pile toe ($l = 0$), the following equations for the axial displacement $w_p(l)$, axial load $P(l)$, and vertical shear stress at the pile shaft $\tau_0(l)$ at a distance l from the pile toe are obtained

$$w_p(l) = w_b \cosh(\mu l) \tag{15}$$

$$P(l) = w_b \mu \pi r_o^2 \lambda G \sinh(\mu l) \tag{16}$$

$$\tau_0(l) = \frac{w_b \mu^2 r_o \lambda G}{2} \cosh(\mu l) \tag{17}$$

$$\frac{P(l)}{w_p(l)} = \mu \pi r_o^2 \lambda G \tanh(\mu l) \tag{18}$$

where $\mu = \sqrt{\frac{2 R^2}{r_o \lambda (r_o \zeta R^2 + t_i)}}$.

4.1.2. Plastic Component

It is assumed that the shear strength at the pile–shaft interface increases linearly with depth, as shown in Equation (19) and Figure 13a. The vertical shear stress ($\tau_0(l)$) along the shaft has already reached the strength value ($\tau_{ult}(l)$).

$$\tau_{ult}(l) = K(b + L - l) \tag{19}$$

where K and b are constants, and L is the pile length as shown in Figure 13a.

Based on Equations (2), (13), (17)–(19), the axial displacement of the pile, $w_p(iL)$ and corresponding load $P(iL)$ at the transition point of iL (the point measured from the pile toe at which the elastic and plastic portions separate; i is the elastoplastic ratio of the remaining elastic portion which is equal to $L1/L$ as shown in Figure 13b) can be expressed as

$$P(iL) = \mu \pi r_o^2 \lambda G \tanh(\mu iL) w_p(iL) \tag{20}$$

$$w_p(iL) = \frac{2}{Gr_o \lambda \mu^2} K[b + L(1 - i)] \tag{21}$$

Within the plastic portion, the pile axial load $P(l)$ at a distance l from the pile toe is

$$P(l) = P(iL) + \int_{iL}^l 2\pi r K(b + L - l) dl \tag{22}$$

Within the plastic portion, the pile axial displacement $w_p(l)$ at a distance l from the pile toe is

$$w_p(l) = w_p(iL) + \int_{iL}^l \frac{P(l)}{\pi r_0^2 \lambda G} dl \tag{23}$$

Combining Equations (20) to (22) then (21) and (22) to (23), the pile axial load $P(L)$ and displacement $w_p(L)$ at the pile head are expressed as

$$P(L) = \frac{2 \pi r_0 \tanh(\mu i L)}{\mu} K[b + L(1 - i)] + \int_{iL}^L 2\pi r K(b + L - l) dl \tag{24}$$

$$w_p(L) = \frac{2}{Gr_0 \lambda \mu^2} K[b + L(1 - i)] + \frac{2 \tanh(\mu i L)}{\mu r_0 \lambda G} K[b + L(1 - i)](L - iL) + \int_{iL}^L \frac{\int_{iL}^l 2\pi r K(b + L - l) dl}{\pi r_0^2 \lambda G} dl \tag{25}$$

An iterative process was developed using *Python* code combined with a *VBA* macro which is presented in Figure 14. This procedure evaluates the load $P(L)$ and displacement $w_p(L)$ at the pile head as head load increases.

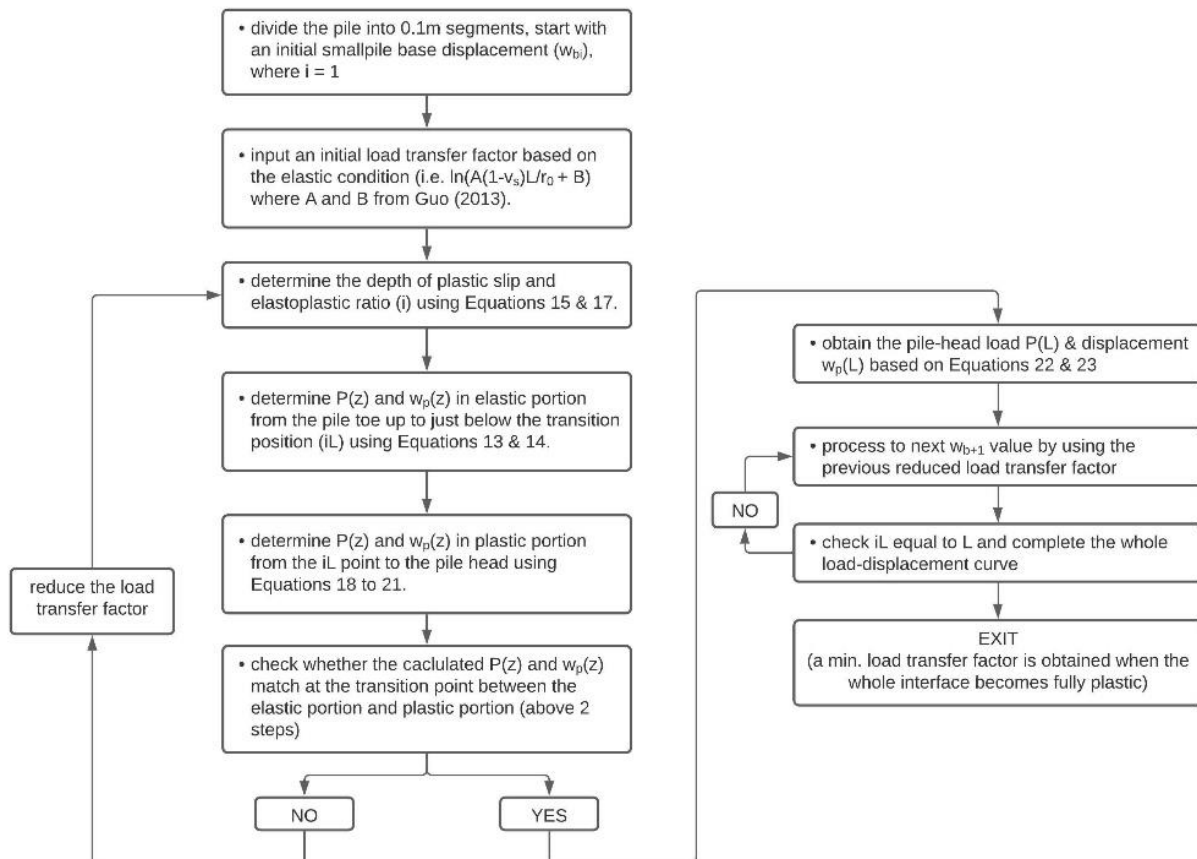


Figure 14. Flowchart for the iterative analytical procedure.

4.2. Improvement in the Load–Displacement Curve at the Pile Head by the New Analytical Method

A total of 44 cases ($L = 10\text{--}30\text{ m}$, $L/r_0 = 40\text{--}60$, $G = 3.8\text{--}7.7\text{ MPa}$, $\nu_s = 0.3$, $\nu_p = 0.15$, $E_p = 30\text{ GPa}$) were analyzed using the analytical method proposed in this paper. This new analytical method considers the change of the load-transfer factor (ζ_{change}) as the pile-head load increases using an automated process; referred to here as the new ζ_{change} analytical method. For comparison, an analysis of the same cases was undertaken using analytical methods that employ a traditional fixed load-transfer factor (ζ_{fixed}) (Section 2.1), which is referred to hereon as the traditional ζ_{fixed} analytical method. The resulting load–displacement curves at the pile head using the different analytical methods (the new ζ_{change} and traditional ζ_{fixed} analytical methods) were compared with FEM results. Figure 15 demonstrates that the new ζ_{change} analytical method (Case 1) yielded results markedly closer to those estimated using FEM than the traditional ζ_{fixed} analytical methods (Case 2). The deviation of the analytical results relative to the FEM results are summarized in Table 3.

Table 3. Summary of percentage deviation from the FE results.

At Head	Numerical	Proposed (Case 1)	Case 2—i	Case 2—ii	Case 2—iii
$P(L)$	8746 kN	+0.5%	−10.2%	−11.0%	−8.3%
$w_p(L)$	54.6 mm	−0.8%	+18.4%	+20.0%	+14.7%

Literature (i), (ii), and (iii) refer to Table 1.

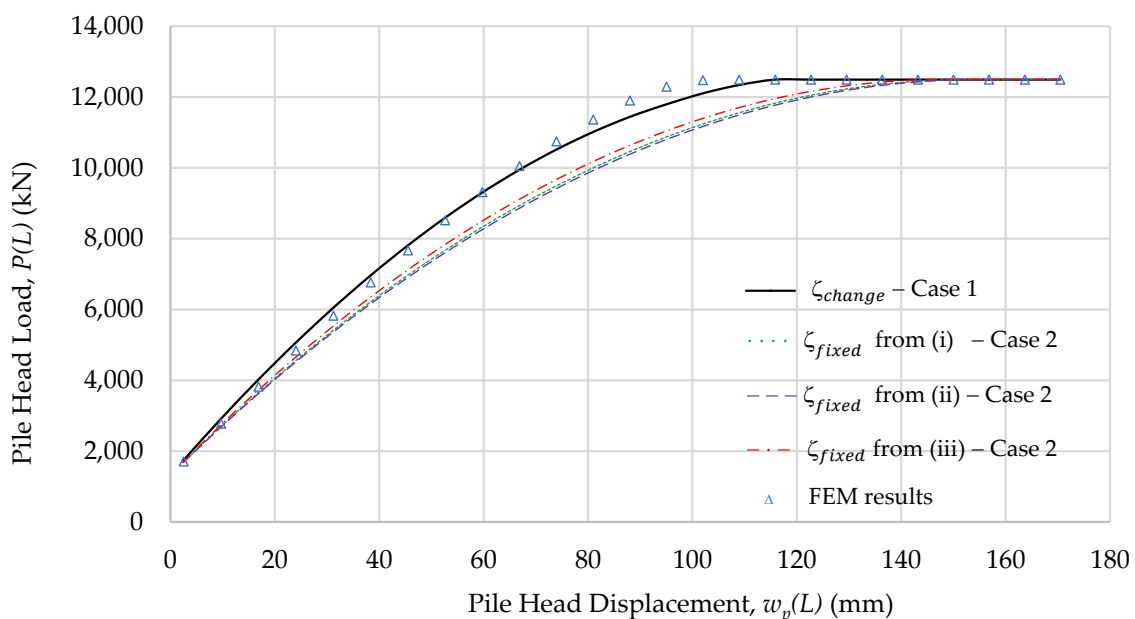


Figure 15. Pile head load versus pile head displacement, improvement of the load–displacement curve ($L = 30\text{ m}$, $L/r_0 = 40$ and $G = 3846\text{ kPa}$).

When applying a factor of safety of 1.5 to the ultimate capacity of the FE result (allowable capacity = 8746 kN), the corresponding pile head displacement is approximately 54.6 mm. Using this displacement as a reference point, the deviation of the head load ($P(L)$) in the analytical solution comparing to the FE analysis estimates is less than +0.5% in Case 1 and a maximum of −11% in Case 2 (using Randolph [11]). To achieve the allowable capacity of 8746 kN, the head displacement deviated −0.8 per cent from the FE analysis result in Case 1, and a maximum of +20.0 per cent in Case 2 (using Randolph [11]). The coefficient of determination (R^2) for all 44 cases is summarized in Figure 16, which shows the new ζ_{change} analytical method has at least a 0.99 correlation with results using FE analysis. In comparison, the traditional ζ_{fixed} analytical method provides a correlation of between 0.91 and 0.95 (using Randolph [11]) with FE analysis results.

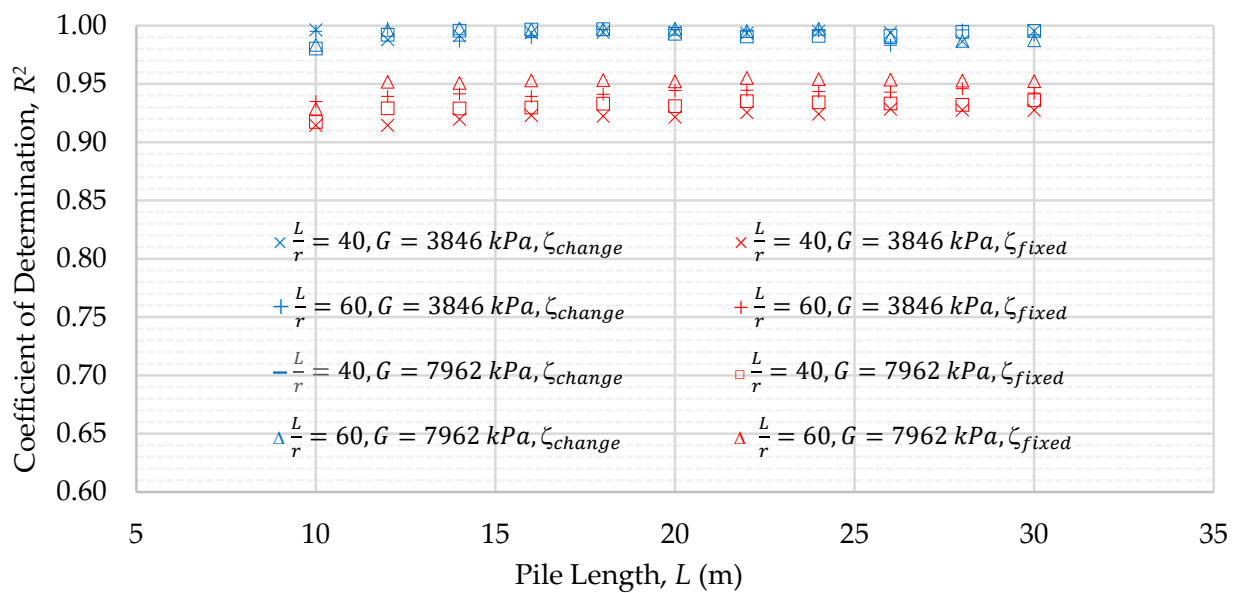


Figure 16. Coefficient of determination (R^2) of load–displacement curves versus pile length (analytical against FE analysis results).

Figures 17–20 show the approximate change of the ζ factors as pile-head load increases in the new ζ_{change} analytical method. The ζ factors versus the pile length are plotted on the right y -axis, with r_m values also provided on the left y -axis for reference. The ζ factors start from an initial maximum value at the purely elastic condition ($\zeta_{elastic}$ can be calculated from the existing literature, Equation (3)). Plastic slip (Figure 10) occurs from the top of the interface when the pile-head load increases and progressively develops down the pile (Figure 13b). The ζ factors reduce and reach a minimum value at the fully plastic condition ($\zeta_{plastic}$). The ζ values at purely elastic and plastic conditions are the upper and lower bounds, respectively. In this study, the maximum reduction in the ζ factors are approximately 40% (80% in r_m values), as pile-head load increases. Figures 17–20 show fluctuations in the minimum values ($\zeta_{plastic}$), which is due to a small deviation of the calculated head load just before the fully plastic condition under the iteration procedure (Case 1 against the FE analysis results in Figure 15). When the pile-head load in the analytical solution is manually adjusted to match the same as the FE results by refining values for ζ , the $\zeta_{plastic}$ values are then straight lines against the pile length (the horizontal dotted lines in Figures 17–20). These lines show that $\zeta_{plastic}$ (the minimum load-transfer factor at the fully plastic condition) is independent of pile length (the dotted lines are horizontal) and independent of the soil shear modulus (the y intercepts of the dotted lines are the same in different soil modulus, i.e., Figure 17 vs. Figure 19), but dependent on the L/r_0 ratio (the y intercepts are different in different L/r_0 ratio, i.e., Figure 17 versus Figure 18). Additionally, the $\zeta_{plastic}$ values increase with the L/r_0 ratio, and this pattern agrees with the $\zeta_{elastic}$ formula proposed under the literature in Equation (3).

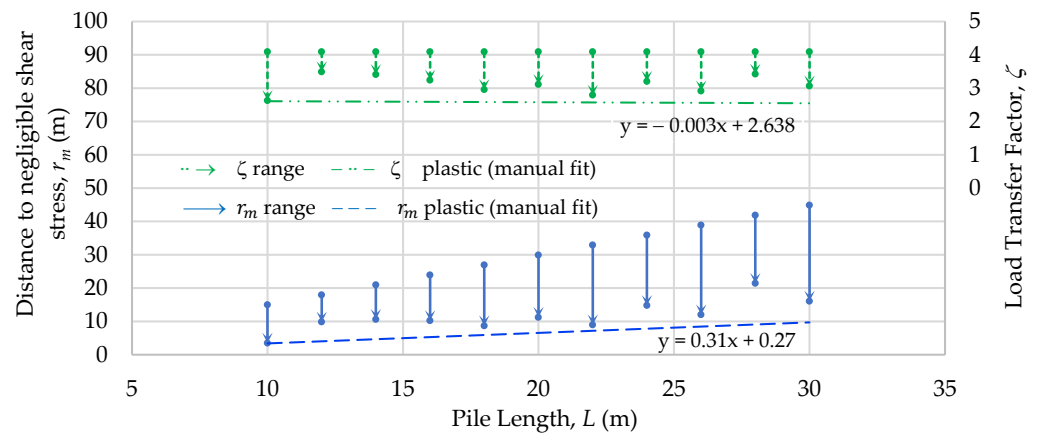


Figure 17. Change of the ζ and r_m values as head load increases (slenderness ratio: $L/r_0 = 40$ and soil shear modulus: $G = 3846$ kPa).

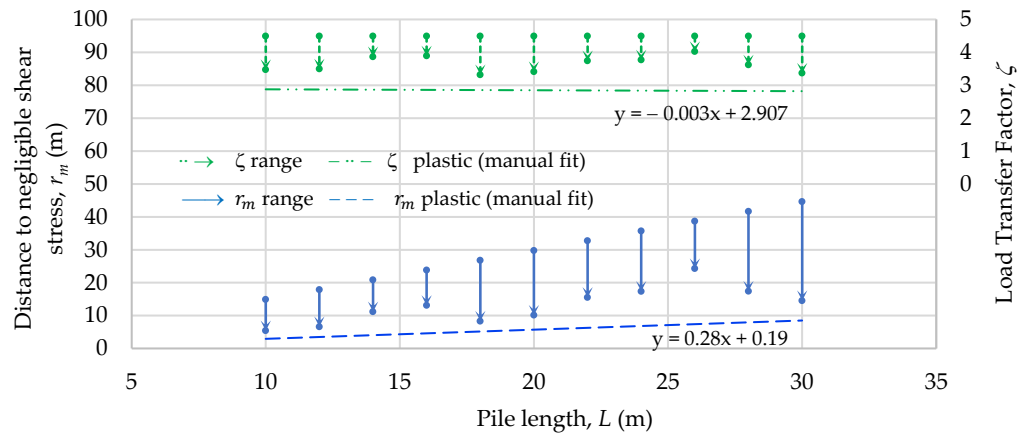


Figure 18. Change of the ζ and r_m values as head load increases (slenderness ratio: $L/r_0 = 60$ and soil shear modulus: $G = 3846$ kPa).

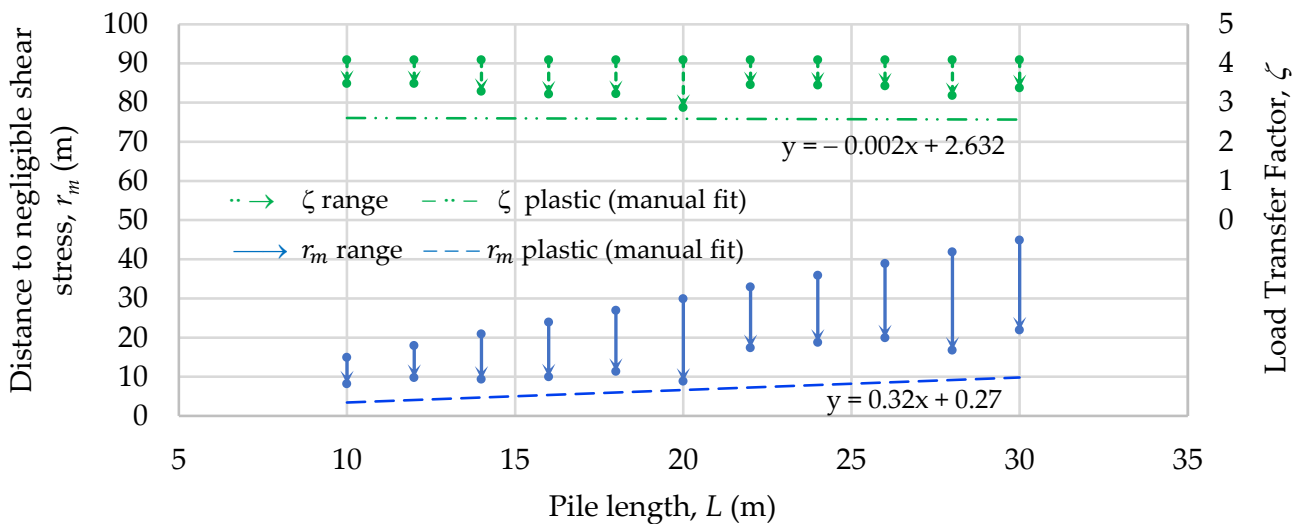


Figure 19. Change of the ζ and r_m values as head load increases (slenderness ratio: $L/r_0 = 40$ and soil shear modulus: $G = 7962$ kPa).

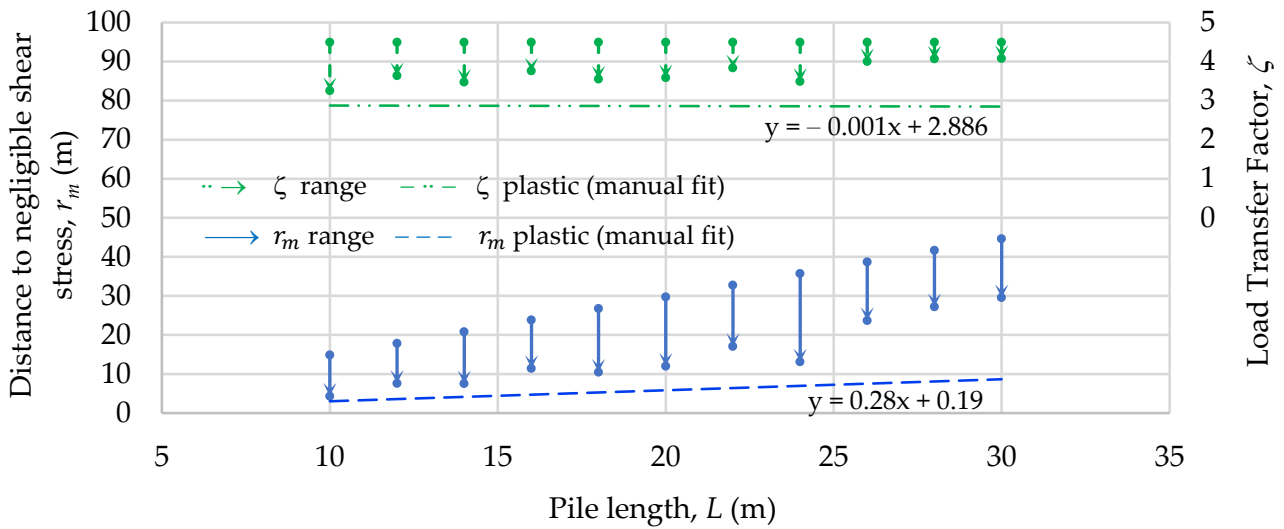


Figure 20. Change of the ζ and r_m values as head load increases (slenderness ratio: $\frac{L}{r} = 60$ and soil shear modulus: $G = 7962$ kPa).

The above scenarios show that load-transfer factor values change with pile head loads (in turn of the elastoplastic ratio, i). Therefore, information on the change and lower bound value ($\zeta_{plastic}$) is necessary to construct the analytical solution. Equations (26) and (27) were developed in a parametric study of over 300 combinations (summarized in Table 4) to match the load–displacement curve between the analytical and FEM results. The same automation using *Python* code and a *VBA* macro described above and in Figure 14 were used to undertake the analyses.

Table 4. Combination of pile geometries and parameters.

L (m)	L/r_0	ν_s	c_{inc} (kPa/m)	G (MPa)
10, 20, 30	20, 40, 60, 80	0.2, 0.3, 0.4	5, 10, 20	2, 6, 15

$$\zeta_{plastic} = \ln \left[0.368 \left(\frac{L}{r_0} \right) \cdot (1 - 0.890 \nu_s) + 3.619 \right] \tag{26}$$

$$\zeta = \ln \left[\frac{0.368 \left(\frac{L}{r_0} \right) \cdot (1 - 0.890 \nu_s) + 3.619}{2.1 \frac{L}{r_0} (1 - \nu_s) + 1} \right] \cdot (1 - i) + \ln \left[2.1 \frac{L}{r_0} (1 - \nu_s) + 1 \right] \tag{27}$$

4.3. Application to a Case Study

A case history is stimulated by adopting the new equations (Equations (24)–(27)) in the new ζ_{change} analytical method. A full-scale test (P1) was carried out by Sowa [28] on a reinforced concrete pile (0.53 m in diameter and 12 m in length) embedded mainly in fine sand with a unit weight of 18.4 kN/m³. Parameters suggested by Zhang et al. [29] were adopted to facilitate later comparison. A soil shear modulus of 2 MPa (average SPT N value of 11) and pile elastic modulus of 30 GPa were adopted, as reported by Zhang et al. [29]. In our new ζ_{change} analytical method, the shear strength profile of the interface (solid line) shown in Figure 21 is adopted such that the ultimate pull-out capacity of 401 kN is achieved. It is the same capacity obtained under Zhang et al. [29] who divides the pile into 12 segments (each approximately 1 m height) with average strength in each segment (dotted line).

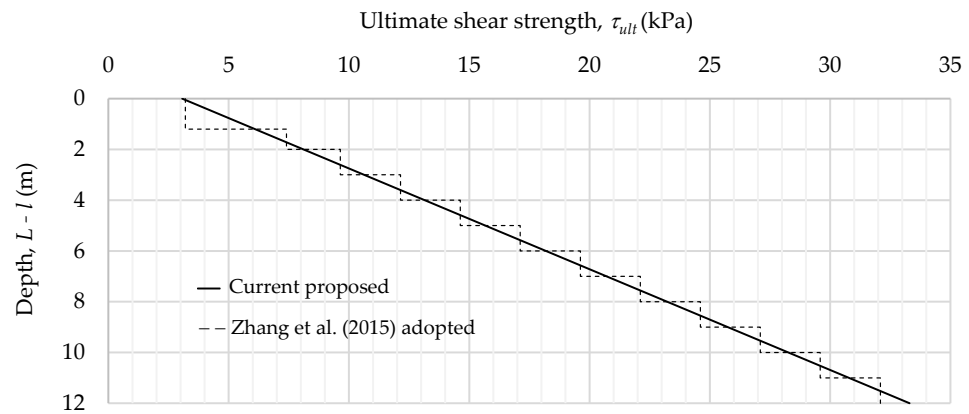


Figure 21. Adopted strength profile of the interface in the proposed analytical and FE models.

The results presented in Figure 22 show a high degree of correlation between the new ζ_{change} analytical method and numerical method (MC model in PLAXIS 2D) for load–displacement estimates. The new ζ_{change} analytical method that considers the change of the load-transfer factor, better agrees with the FEM results compared to the results from the traditional fixed factor (ζ_{fixed}). Furthermore, it shows an improvement from Zhang et al. (2015) when their suggested parameters are adopted. However, the proposed analytical method slightly underestimates the initial load–displacement curve and overestimates the portion just before the interface becomes fully plastic (compared to the measured field data). This is a disadvantage of the linear-elastic-perfectly-plastic behavior in the Mohr–Coulomb (MC) model. To address this, a non-linear stress-dependent modulus was used in the hyperbolic form of

$$G = G_0 \left(1 - \frac{\tau_0}{\tau_{ult}} \right) \tag{28}$$

where G_0 is the initial shear modulus, $G_0 = G_{50} / (1 - R_f/2)$, R_f is the ratio of the maximum allowable shear stress to the asymptotic value in the hyperbolic form, and G_{50} is assumed the same as the soil shear modulus adopted in the MC model. Using this hyperbolic function improved these two portions of the load–displacement curve as shown in Figure 23.

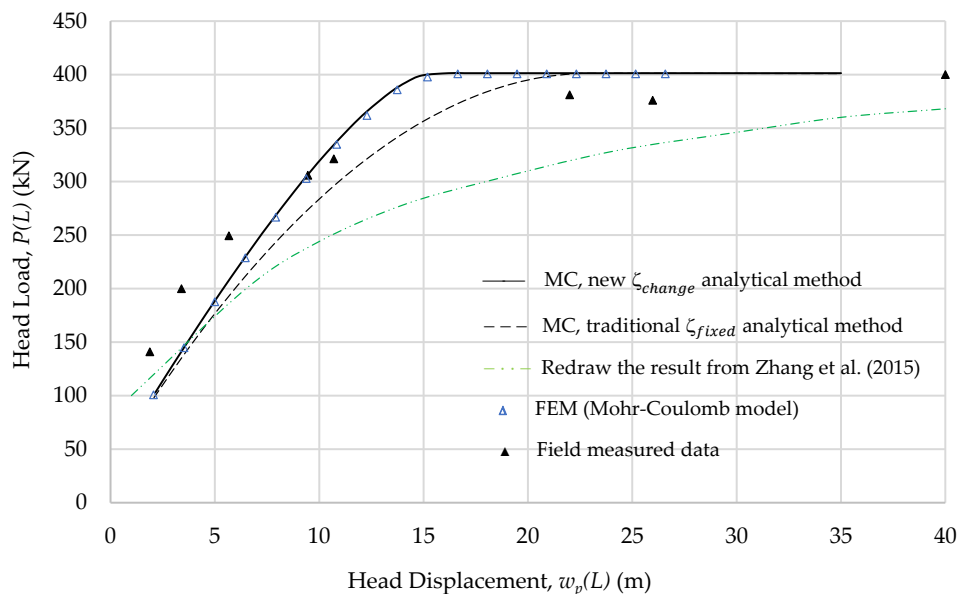


Figure 22. Load–displacement curve at the pile head in the case study P1 of Sowa [28].

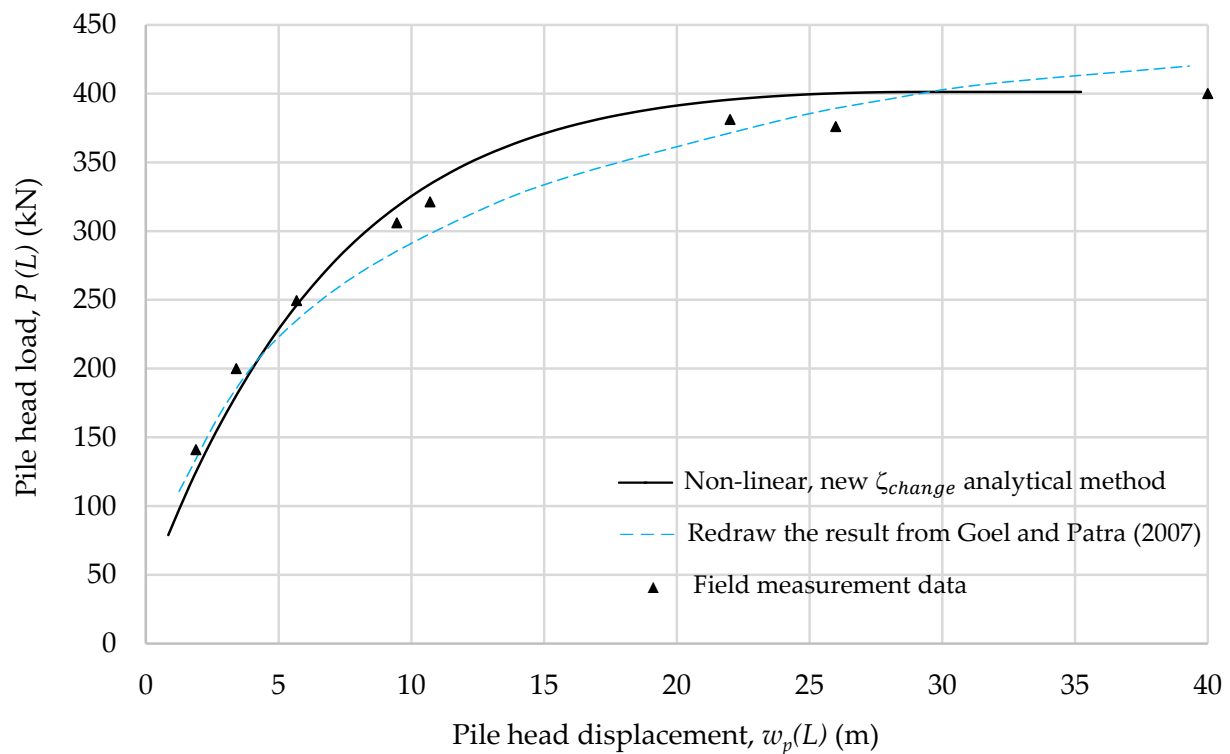


Figure 23. Further improvement by using a nonlinear hyperbolic analytical model.

5. Conclusions

Many researchers have considered the pile–soil slipping theory in the analytical method by introducing an interface in the analytical formulation that allows relative displacement between the pile and soil surfaces. It is similar to many rigorous numerical methods that adopt interface elements to simulate the pile–soil slipping behaviors to achieve more accurate and realistic results. This study investigated the use of the existing load-transfer factor (a constant value during pile loading and devised under the elastic soils) in slipping analytical models and found deviation in the load–displacement results as explained by mathematical theories and numerical results. It draws attention to the use of the existing load-transfer factor in the slipping analytical theory. The study shows a constant ζ factor is valid in elastic soils and soils with a constant ratio of shear modulus to strength in the Gibson condition for axially loaded piles. Some cohesionless soils are characterized by the pile–soil plastic slip commencing at the upper portion of the pile shaft and progressively developing down the pile. It is found that the ζ factor changes as pile-head load increases in these soils. To address this, a new equation for the load-transfer factor and a new analytical method to develop the load–displacement curve are proposed to improve the slipping analytical method in these soils. Using the new equation and analytical method, the results demonstrate that the load–displacement curve is improved and correlates well with corresponding Mohr–Coulomb models in the FEM. The study results suggested that the change of the ζ factor is independent of soil modulus, and therefore, it is expected to apply to nonlinear soils. Therefore, further research and verification based on this fundamental study expanding to nonlinear models are recommended for continuous improvement.

Author Contributions: Conceptualization by K.L. and E.O.; Methodology, K.L. and E.O.; Software, K.L.; Validation, K.L.; Formal analysis, K.L.; Investigation, K.L.; Resources, K.L., D.N. and C.Y.; Data curation, K.L.; Writing—original draft preparation, K.L.; Writing—review and editing, K.L., E.O., D.N. and C.Y.; Visualization, K.L.; Supervision, E.O.; Project administration, E.O. and C.Y. All authors have read and agreed to the published version of the manuscript.

Funding: This research received no external funding.

Institutional Review Board Statement: Not applicable.

Informed Consent Statement: Not applicable.

Data Availability Statement: The data that support the findings of this study are available from the corresponding author upon reasonable request.

Conflicts of Interest: The authors declare no conflict of interest.

References

1. Randolph, M.F.; Wroth, C.P. Analysis of deformation of vertically loaded piles. *J. Geotech. Geoenviron. Eng.* **1978**, *104*, 1465–1488. [[CrossRef](#)]
2. Kraft, L.M.; Ray, R.P.; Kagawa, T. Theoretical t-z curves. *J. Geotech. Geoenviron. Eng.* **1981**, *107*, 1543–1561. [[CrossRef](#)]
3. Alawneh, A.S. Modelling load-displacement response of driven piles in cohesionless soils under tensile loading. *Comput. Geotech.* **2005**, *32*, 578–586. [[CrossRef](#)]
4. Pando, M.A.; Ealy, C.D.; Filz, G.M.; Lesko, J.J.; Hoppe, E.J. *A Laboratory and Field Study of Composite Piles for Bridge Substructures*; Federal Highway Administration, United States: Washington, DC, USA, 2006.
5. Wang, Z.; Xie, X.; Wang, J. A new nonlinear method for vertical settlement prediction of a single pile and pile groups in layered soils. *Comput. Geotech.* **2012**, *45*, 118–126. [[CrossRef](#)]
6. Zhang, Q.Q.; Li, S.C.; Zhang, Z.M. Influence of reaction piles on test pile response in a static load test. *J. Zhejiang Univ. Sci. A* **2013**, *14*, 198–205. [[CrossRef](#)]
7. Cheng, S.; Zhang, Q.Q.; Li, S.C.; Li, L.P.; Zhang, S.M.; Wang, K. Nonlinear analysis of the response of a single pile subjected to tension load using a hyperbolic model. *Eur. J. Environ. Civ. Eng.* **2018**, *22*, 181–191. [[CrossRef](#)]
8. Lo, K.; Newell, D.; Oh, E. Comparing analytical models with slipping and non-slipping interface in axially loaded tension piles. In Proceedings of the 45th Annual Conference on Deep Foundations Institute, Online Conference, 27–30 October 2020.
9. Sheil, B.B.; McCabe, B.A. An analytical approach for the prediction of single pile and pile group behaviour in clay. *Comput. Geotech.* **2016**, *75*, 145–158. [[CrossRef](#)]
10. Boonyatee, T.; Lai, Q.V. A non-linear load transfer method for determining the settlement of piles under vertical loading. *Int. J. Geotech. Eng.* **2017**, *14*, 206–217. [[CrossRef](#)]
11. Randolph, M.F. Design methods for pile group and piled rafts. In Proceedings of the 13th International Conference of Soil Mechanics and Foundation Engineering, New Delhi, India, 5–10 January 1994; pp. 61–82.
12. Poulos, H.G.; Davis, E.H. *Pile Foundation Analysis and Design*; John Wiley & Sons Inc.: Hoboken, NJ, USA, 1980.
13. Carter, J.P.; Kulhawy, F.H. *Analysis and Design of Drilled Shaft Foundations Socketed into Rock*; Electric Power Research Inst.: Palo Alto, CA, USA; Cornell Univ.: Ithaca, NY, USA, 1988; pp. 1943–1944.
14. Guo, W.D. *Theory and Practice of Pile Foundations*; Taylor & Francis Group: New York, NY, USA, 2013.
15. De Gennaro, V.; Frank, R.; Said, I. Finite element analysis of model piles axially loaded in sands. *Riv. Ital. Geotech.* **2008**, *2*, 44–62.
16. Boulon, M. Basic features of soil structure interface behaviour. *Comput. Geotech.* **1989**, *7*, 115–131. [[CrossRef](#)]
17. Selvadurai, A.P.S. Boundary element modelling of geomaterial interfaces. In *Mechanics of Geomaterial Interfaces*; Selvadurai, A.P.S., Boulon, M.J.B., Eds.; Elsevier: Amsterdam, The Netherlands, 1995; Volume 42, pp. 173–197.
18. Coutinho, A.L.G.A.; Martins, M.A.D.; Sydenstricker, R.M.; Alves, J.L.D.; Landau, L. Simple zero thickness kinematically consistent interface elements. *Comput. Geotech.* **2003**, *30*, 347–374. [[CrossRef](#)]
19. Reddy, E.S.; Chapman, D.N.; Sastry, V. Direct shear interface test for shaft capacity of piles in sand. *Geotech. Test. J.* **2000**, *23*, 199–205.
20. Damians, I.P.; Yub, Y.; Lloret, A.; Bathurst, R.J.; Josa, A. Equivalent interface properties to model soil-facing interactions with zero-thickness and continuum element methodologies. In Proceedings of the 15th Pan-American Conference on Soil Mechanics and Geotechnical Engineering, Buenos Aires, Argentina, 15–18 November 2015; pp. 1065–1072.
21. Wu, J.J.; Li, Y.; Cheng, Q.G.; Wen, H.; Liang, X. A simplified method for the determination of vertically loaded pile-soil interface parameters in layered soil based on FLAC 3D. *Front. Struct. Civ. Eng.* **2016**, *10*, 103–111. [[CrossRef](#)]
22. PLAXIS 2D. *PLAXIS 2D Reference Manual CONNECT Edition V20*; Plaxis bv, Bentley System, Inc.: Delft, The Netherlands, 2019.
23. Das, B.M. Uplift capacity of piles and pile groups in sand. In Proceedings of the Oceans’ 86, Washington, DC, USA, 22 January 1999; pp. 90–95.
24. O’Neill, M.W. Side resistance in piles and drilled shafts. *J. Geotech. Geoenviron. Eng.* **2001**, *127*, 3–16. [[CrossRef](#)]
25. De Nicola, A.; Randolph, M.F. Tensile and compressive shaft capacity of piles in sand. *J. Geotech. Eng.* **1993**, *119*, 1952–1973. [[CrossRef](#)]
26. Misra, A.; Chen, C.H.; Oberoi, R.; Kleiber, A. Simplified analysis method for micropile pullout behavior. *J. Geotech. Geoenviron. Eng.* **2004**, *130*, 1024–1033. [[CrossRef](#)]
27. Meerdink, L.A. Performance of Micropiles under Axial Tensile Loading. Master’s Thesis, Delft University of Technology, Delft, The Netherlands, 2013.

-
28. Sowa, V.A. Pulling capacity of concrete cast in situ bored piles. *Can. Geotech. J.* **1970**, *7*, 482–493. [[CrossRef](#)]
 29. Zhang, Q.Q.; Li, S.C.; Zhang, Q.; Li, L.P.; Zhang, B. Analysis on response of a single pile subjected to tension load using a softening model and a hyperbolic model. *Mar. Georesour. Geotechnol.* **2015**, *33*, 167–176. [[CrossRef](#)]